



Berry curvature induced linear electro-optic effect in chiral topological semimetalsZhi Li,^{1,*} Yuewen Gao,¹ Yu Gu,¹ Shengli Zhang,¹ Toshiaki Iitaka² ,² and W. M. Liu^{3,†} ¹*MIT Key Laboratory of Advanced Display Materials and Devices, School of Materials Science and Engineering, Nanjing University of Science and Technology, Nanjing 210094, China*²*Discrete Event Simulation Research Team, RIKEN Center for Computational Science, 2-1 Hirosawa, Wako, Saitama 351-0198, Japan*³*Beijing National Laboratory for Condensed Matter Physics and Institute of Physics, Chinese Academy of Sciences, Beijing 100190, China*

(Received 26 October 2021; revised 25 November 2021; accepted 8 March 2022; published 21 March 2022)

We studied the linear electro-optic effect of chiral topological semimetals which are characterized by high-fold chiral fermions separated in energy space. We identify that the general second-order conductivity $\sigma_{xyz}^{(2)}(\omega)$ includes three sources from the shift current, injection current, and nonlinear anomalous current with frequency ω , respectively. The $\sigma_{xyz}^{(2)}(\omega)$ contributed by the nonlinear anomalous current is antisymmetric under the exchange of indices x and y , and it is proportional to relaxation time and Chern number. We demonstrate that the electro-optic coefficient below 0.65 eV in chiral crystal RhSi is dominated by the nonlinear anomalous current and injection current, and it renders a relatively low half-wave voltage in the order of hundreds of volts. This work classifies how the Berry curvature modifies the linear electro-optic effect in chiral topological semimetals and opens an avenue to design the electro-optic modulator with half-wave voltage compatible with the complementary metal-oxide semiconductor circuit.

DOI: [10.1103/PhysRevB.105.125201](https://doi.org/10.1103/PhysRevB.105.125201)**I. INTRODUCTION**

Transition metal silicides CoSi, RhSi, and PdGa crystallize into a simple cubic structure with space group $P2_13$ [1] which includes no spatial inversion symmetry or mirror symmetry, and they afford an excellent platform for the realization of high-fold chiral fermions [2–4]. In the band structure of RhSi by calculation and angle-resolved photoelectron spectroscopy (ARPES) experiments [5–8], the spin-1 fermion at the Γ point and the topological charge-2 fermion at the R point are separated in energy scale because of absent mirror symmetry. The absolute magnitude of the Chern number with the Berry curvature around the Γ point is determined to 2 in CoSi and RhSi by ARPES measurements [9–11]. However, higher Chern number $C = 4$ is observed in PdGa which has much stronger spin-orbital coupling (SOC) [12,13]. Except for the novel high-fold chiral fermions in chiral topological semimetal RhSi, photogalvanic effect is also widely studied for potential application in the field of infrared or terahertz detection [14–19], and possible quantized circular photogalvanic effect (CPGE) [20–23]. Experimentally, the CPGE in the chiral topological semimetal RhSi is observed in an energy window below 0.65 eV [24–26], where the CPGE contributed from both chiral fermions with opposite chiral chirality will not be canceled out.

The linear electro-optic effect [27–30], is essentially a second-order response under optical signal with high frequency and electric signal with low frequency [31–38]. The general formalism for the second-order optical response of

solids was proposed by Sipe and Shkrebti [39]. The lengthy formalism for the electro-optic coefficient, which includes intraband and interband contributions, applies to a semiconductor under light field with photon energy $\hbar\omega < E_g$ (E_g band gap). However, this requirement cannot be fulfilled in chiral topological semimetals. A new theory for electro-optic effect in topological semimetals should be developed. In the community of topological quantum matters, the low energy band dispersion near the Fermi level is classified by different fermions carrying a Chern number [40–43]. Specifically, the linear band crossing plays the role of source or sink of Berry curvature. The new theory should also clarify how the Berry curvature or quantum geometric tensor affects the electro-optic effect. Since the Berry curvature in chiral topological semimetals is distributed in different energy scales, the chiral topological semimetals offer an excellent platform to investigate how the Berry curvature modifies the linear electro-optic effect and propagation of the optical signal.

In this work, we studied the linear electro-optic effect in chiral topological semimetals. We identify that all the oscillating currents with frequency ω from the shift current, injection current, and nonlinear anomalous current can modify the refractivity of chiral topological semimetals. For a clean single crystal with long relaxation time, the nonlinear anomalous current resulting from the topologically nontrivial bands is dominating. The $\sigma_{xyz}^{(2)}(\omega)$ contributed by the nonlinear anomalous current is antisymmetric under the exchange of indices x and y , and it is proportional to relaxation time. By numerical calculation, we demonstrate that the giant electro-optic coefficient in chiral crystal RhSi is dominated by the nonlinear anomalous current and injection current below 0.65 eV, and it renders a relatively low half-wave voltage in the order of hundreds of volts.

*zhili@njust.edu.cn

†wmliu@iphy.ac.cn

II. NONLINEAR CURRENTS

We start from the light-matter interaction $H = h_0 - e\vec{E}(t) \cdot \vec{r}$ within the dipole approximation [44,45], in which h_0 describes the ground state and $\vec{E}(t)$ is the external field including both optical and electric signals. The velocity operator reads $\vec{v}(t) = \frac{i}{\hbar}[H, \vec{r}(t)]$ in which position operator $\vec{r}(t) = e^{-iHt/\hbar}\vec{r}e^{-iHt/\hbar}$. The Bloch function satisfies $h_0|n(\vec{k})\rangle = \varepsilon_n(\vec{k})|n(\vec{k})\rangle$, and the position matrix reads $\vec{r}_{nm}(\vec{k}) = \vec{A}_{nm}(\vec{k}) + i\delta_{nm}\partial_{\vec{k}}$ in which $\vec{A}_{nm}(\vec{k}) = i\langle n(\vec{k})|\partial_{\vec{k}}|m(\vec{k})\rangle$ is the Berry connection between bands n and m at momentum \vec{k} . The current density reads $\vec{j}(t) = -e\langle\psi(\vec{r}, t)|\vec{v}(t)|\psi(\vec{r}, t)\rangle$, in which the field operator $\psi(r, t)$ can be expanded by Bloch functions. Further, we introduce density operator $\rho(t) = |\psi(t)\rangle\langle\psi(t)|$, and calculate the density matrix $\rho_{nm}(\vec{k}) = \langle n(\vec{k})|\rho(t)|m(\vec{k})\rangle = \rho_{nm}^{(0)}(\vec{k}) + \rho_{nm}^{(1)}(\vec{k}) + \rho_{nm}^{(2)}(\vec{k}) + \dots$ by equation $i\hbar\frac{d\rho(t)}{dt} = [H, \rho(t)]$ in which the constant relaxation time τ is absorbed into frequency $(\omega - i\tau^{-1})$. The zero-order $\rho_{nm}^{(0)}(\vec{k})$ is the Fermi-Dirac distribution for band m . After some lengthy but straightforward calculations, the second-order response contributed oscillating current $\vec{j}^{(2)}(\omega)$ with frequency ω reads

$$\begin{aligned} j^{(2),u}(\omega) &= j_{\text{intra}}^u(\omega) + j_{\text{inter}}^u(\omega) + j_{BCD}^u(\omega) \\ &= \sum_{\omega_1, \omega_2} \sigma_{ijk}^{(2)}(\omega) E_j(\omega_1) E_k(\omega_2) \delta(\omega, \omega_1 + \omega_2), \quad (1) \end{aligned}$$

where frequency-dependent second-order conductivity $\sigma_{ijk}^{(2)}(\omega; \omega_1, \omega_2) = \alpha_{ijk}(\omega; \omega_1, \omega_2) + i\beta_{ijk}(\omega; \omega_1, \omega_2)$. The first term α_{ijk} is symmetric under the exchange of j and k , while the second term β_{ijk} is antisymmetric under the exchange of j and k . The oscillating current $\vec{j}^{(2)}(\omega)$ includes three sources from intraband and interband contributions. The intraband contribution $j_{\text{intra}}^u(\omega) = -e \int d\vec{k} v_{mn}^u \rho_{nn}^{(2)}(\vec{k}, \omega)$ reads

$$\begin{aligned} j_{\text{intra}}^u(\omega) &= \frac{e^3 \hbar^{-1}}{\hbar\omega - i\eta} \sum_{mn} \sum_{\omega_1, \omega_2} \int d\vec{k} \delta(\omega, \omega_1 + \omega_2) \\ &\times \frac{\partial \varepsilon_{nm}(\vec{k})}{\partial k^u} \frac{Q_{mn}^{ij}(\vec{k}) [\rho_{mm}^{(0)} - \rho_{nn}^{(0)}]}{\hbar\omega_2 - \varepsilon_{nm}(\vec{k}) - i\eta} E_i(\omega_1) E_j(\omega_2), \quad (2) \end{aligned}$$

where $\varepsilon_{nm}(\vec{k}) = \varepsilon_n(\vec{k}) - \varepsilon_m(\vec{k})$ and $\eta = \hbar/\tau$. The interband quantum geometric tensor [46–50] $Q_{mn}^{ij}(\vec{k}, \omega) = \Gamma_{mn}^{ij}(\vec{k}, \omega_2) + i\Omega_{mn}^{ij}(\vec{k}, \omega_2)$ is defined as

$$\begin{aligned} 2\Gamma_{mn}^{ij}(\vec{k}) &= A_{mn}^i(\vec{k}) A_{nm}^j(\vec{k}) + \text{c.c.}, \\ 2i\Omega_{mn}^{ij}(\vec{k}) &= A_{mn}^i(\vec{k}) A_{nm}^j(\vec{k}) - \text{c.c.} \quad (3) \end{aligned}$$

The metric tensor $\Gamma_{mn}^{ij}(\vec{k})$ and curvature tensor $\Omega_{mn}^{ij}(\vec{k})$ are even and odd functions of momentum \vec{k} , respectively. If the time-reversal invariant symmetry is preserved, only the curvature involved contribution will be kept. This intraband contribution is also dubbed as injection current in photogalvanic effect. However, we focus on ac $j_{\text{intra}}^u(\omega)$ in linear electro-optic effect, instead of dc $j_{\text{intra}}^u(0)$ in photogalvanic effect. The

interband contribution $j_{\text{inter}}^u(\omega) = -e \int d\vec{k} v_{mn}^u \rho_{nm}^{(2)}(\vec{k}, \omega)$ reads

$$\begin{aligned} j_{\text{inter}}^u(\omega) &= e^2 \sum_{mn} \sum_{\omega_1, \omega_2} \int d\vec{k} \delta(\omega, \omega_1 + \omega_2) \\ &\times v_{mn}^u \frac{\vec{E}(\omega_1) \cdot \vec{D}(\vec{k}) \rho_{nm}^{(1)}(\vec{k}, \omega_2)}{\hbar\omega - \varepsilon_{nm}(\vec{k}) - i\eta}, \quad (4) \end{aligned}$$

where the interband velocity $\vec{v}_{mn}(\vec{k}) = i\hbar^{-1} \varepsilon_{nm}(\vec{k}) \vec{A}_{mn}(\vec{k})$, and the first-order interband matrix $\rho_{nm}^{(1)}(\vec{k}, \omega) = \frac{-e\vec{E}(\omega) \vec{A}_{nm}(\vec{k})}{\hbar\omega - \varepsilon_{nm}(\vec{k}) - i\eta} (\rho_{mm}^{(0)} - \rho_{nn}^{(0)})$. The shift vector $\vec{D}(\vec{k}) = i\partial_{\vec{k}} + A_{nn}(\vec{k}) - A_{mm}(\vec{k})$ plays the role of a covariant derivative, and it characterizes the difference between intracell position matrices within valence (hole) and conduction bands (electron). This interband contribution is also dubbed as shift current in photogalvanic effect, and dominating in semiconducting materials [51]. The second-order optical conductivity contributed by shift current $j_{\text{inter}}^u(\omega)$ has to be estimated by the first-principles calculation. The other term from interband contribution reads

$$\begin{aligned} j_{BCD}^u(\omega) &= \frac{e^3}{\hbar} \sum_{mn} \sum_{\omega_1, \omega_2} \int d\vec{k} \frac{\varepsilon_{mn}(\vec{k}) E_i(\omega_1) E_j(\omega_2)}{\hbar\omega - \varepsilon_{nm}(\vec{k}) - i\eta} \\ &\times [\Gamma_{mn}^{ui}(\vec{k}) + i\Omega_{mn}^{ui}(\vec{k})] \frac{\partial_{k^j} [\rho_{mm}^{(0)} - \rho_{nn}^{(0)}(\vec{k})]}{\hbar\omega_2 - i\eta}. \quad (5) \end{aligned}$$

This term is contributed by the generalized Berry curvature dipole [52,53] in the case of a multiple bands system, and dubbed as nonlinear anomalous current. Similar to the injection current, only the curvature involved contribution will keep in nonlinear anomalous current if time-reversal invariant symmetry is preserved. If we constrain $\omega = 0$, Eq. (1) describes the photogalvanic effect. If we constrain $\omega_1 = 0$, or $\omega_2 = 0$, but $\omega_1 + \omega_2 = \omega$, Eq. (1) describes the linear electro-optic effect. The detailed derivation of Eq. (1) by a density matrix method is present in the Supplemental Material [54]. In the case of resonance, i.e., $\hbar\omega = \varepsilon_{nm}(\vec{k})$, the intraband current is reduced to

$$j_{\text{intra}}^u(\omega) = \frac{\pi e^3 \hbar^{-1}}{\hbar\omega - i\eta} \sum_m \int d\vec{k} \partial_{k^u} \Omega_{mm}^{ij}(\vec{k}) E_i(0) E_j(\omega),$$

while the nonlinear anomalous current in Eq. (5) is reduced to

$$j_{BCD}^u(\omega) = \frac{-i\tau\pi e^3}{\hbar^2} \sum_m \oint d\vec{k} \partial_{k^j} \Omega_{mm}^{ui}(\vec{k}) E_i(\omega) E_j(0),$$

in which the integral should be performed on the isoenergetic surface satisfying $\hbar\omega = \varepsilon_{nm}(\vec{k})$ surrounding the source or sink of Berry curvature, and m (n) should be one occupied (unoccupied) band index. The ratio between $j_{BCD}^u(\omega)$ and $j_{\text{intra}}^u(\omega)$ is $|\omega\tau - i|$, i.e., $j_{BCD}^u(\omega)$ will be dominating if $\omega\tau \gg 1$. In the case of two bands, the interband curvature $2|\Omega_{mn}|$ is reduced to Berry curvature of band m behaving like $\frac{\chi}{2}|k|^{-2}$ near the source or sink, and both $j_{\text{intra}}^u(\omega)$ and $j_{BCD}^u(\omega)$ are proportional to the topological charge or Chern number χ . With the applied optical signal in the xy plane and the electric signal along the z direction as shown in Fig. 1(a), the second-order optical conductivity $\sigma_{xyz}(\omega) = j_{BCD}^x(\omega)/[E_y(\omega)E_z]$ from Eq. (5) reads $\frac{i\chi\tau e^3}{2\hbar^2}$, and $\sigma_{xyz}(\omega) = -\sigma_{yxz}(\omega)$. With $\tau = 1$ fs and $\chi = 2$, the

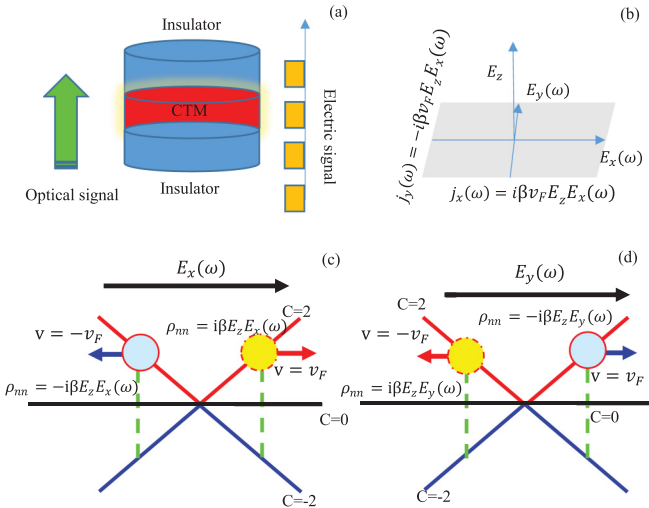


FIG. 1. (a) Schematic diagram for the electro-optic modulator consisting of chiral topological matter (CTM) and insulating cladding layers. (b) Nonlinear Hall current induced by Berry curvature, indicating the nonlinear Hall coefficient is antisymmetric. (c),(d) Schematic diagrams for carrier generation and electronic velocity in momentum space, where β is a real coefficient. The Chern number of each band is labeled by C .

$\sigma_{xyz}(\omega) = 9.33 \mu\text{A}/\text{V}^2$. The microscopic picture is shown in Figs. 1(b)–1(d) in which both velocity and carrier density are odd functions of momentum.

III. ELECTRO-OPTIC EFFECT

So far, we have clarified the three sources for second-order optical conductivity in chiral topological matter. We should further clarify how the nonlinear current changes the propagation of the optical signal in chiral topological matter. We take the RhSi as an example, and consider a light beam with propagating vector q along the z direction and linear polarization in the xy plane, and an applied (static or low frequency) bias voltage along the z direction. For monochromatic light with a frequency of ω , the total electron current oscillating with a frequency of ω reads $j_i(\omega) = \sigma_{ij}(\omega)E_j(\omega) + j_i^{(2)}(\omega)$, in which the first term is contributed by the linear response including both intraband and interband contributions. From Eq. (1), the nonlinear Hall current with frequency ω reads

$$\begin{aligned} j_x^{(2)}(\omega) &= \sigma_{xyz}^{(2)}(\omega; \omega, 0)E_z E_y(\omega), \\ j_y^{(2)}(\omega) &= \sigma_{xyz}^{(2)*}(\omega; \omega, 0)E_z E_x(\omega). \end{aligned} \quad (6)$$

For the chiral topological semimetal RhSi with space group $P2_13$ (No. 198), the only nonvanishing elements of second-order conductivity $\sigma_{ijk}^{(2)}$ have indices xyz and its permutations. From the macroscopic equations of Maxwell's equations, the complex refractive index $\tilde{N}(\omega) = \frac{c\omega}{\omega}$ (c the speed of light in vacuum) satisfies

$$\begin{pmatrix} \tilde{N}^2 - N^2(\omega) & \sigma_{xyz}^{(2)} E_z \\ \sigma_{xyz}^{(2)*} E_z & \tilde{N}^2 - N^2(\omega) \end{pmatrix} \begin{pmatrix} E_x(\omega) \\ E_y(\omega) \end{pmatrix} = 0, \quad (7)$$

in which $N^2(\omega) = \epsilon(\omega)$ and $\epsilon(\omega)$ is the complex dielectric tensor from linear response theory. The two solutions for

$\tilde{N}(\omega)$ read

$$\tilde{N}_{\pm}(\omega) = \sqrt{N^2(\omega) \pm |\chi_{xyz}^{(2)}(\omega; \omega, 0)| E_z}, \quad (8)$$

and $\sigma_{xyz}^{(2)}(\omega; \omega, 0) = -i\omega\epsilon_0\chi_{xyz}^{(2)}(\omega; \omega, 0)$. The two eigenvectors $\frac{1}{\sqrt{2}}|E(\omega)\rangle(1, \pm 1)$ can be interpreted as two orthogonal optical fields with different polarizations, and $|E(\omega)\rangle e^{-\omega\tilde{N}_{\pm}z/c}$ is the strength of the propagating electromagnetic wave. Equation (8) also demonstrates that the two orthogonal optical fields in chiral crystal have different refractivities $\tilde{n}_{\pm}(\omega) = \text{Re}\tilde{N}_{\pm}(\omega)$. From Eq. (8), the difference between $\tilde{n}_{+}(\omega)$ and $\tilde{n}_{-}(\omega)$ reads

$$\Delta n(\omega) = \tilde{n}_{+}(\omega) - \tilde{n}_{-}(\omega) \sim \frac{|\chi_{xyz}^{(2)}(\omega; \omega, 0)| E_z}{2n(\omega)}, \quad (9)$$

in which $n(\omega)$ is the real part of the complex index of refraction $N(\omega)$ from linear response theory. After a light beam passes through the electro-optic crystal, the phase difference between the two orthogonal optical fields is given by

$$\Delta\varphi = \Delta n(\omega) \frac{\omega L}{c}, \quad (10)$$

in which L is the length of the crystal along the z direction which is parallel to the propagating vector of the light field. The half-wave voltage is given by

$$V_{\lambda/2} = \frac{2\pi n(\omega)c}{\omega |\chi_{xyz}^{(2)}(\omega; \omega, 0)|}. \quad (11)$$

IV. NUMERICAL RESULTS AND DISCUSSION

To determine the frequency-dependent half-wave voltage, we need the information of refractivity $n(\omega)$ and $\chi_{xyz}^{(2)}(\omega; \omega, 0)$. Both refractivity $n(\omega)$ and $\chi_{xyz}^{(2)}(\omega; \omega, 0)$ can be calculated by the first-principles calculation based on density functional theory. In this work, the linear optic properties of RhSi are calculated by all-electron full-potential linearized augmented plane wave (LAPW) code ELK [55], while the second-order susceptibility $\chi_{xyz}^{(2)}(\omega; \omega, 0)$ contributed by a shift vector mechanism is calculated by the ABINIT code with sum-over-state approximation [56,57]. Lastly, the frequency-dependent half-wave voltage is calculated by Eq. (11).

Since the SOC effect is weak in chiral topological semimetal RhSi, we ignore the SOC effect in the first-principles calculation and adopt fine k -point grids $50 \times 50 \times 50$ for linear optic properties with intraband contribution (Drude term). The calculated band structure is shown in Fig. 2(a), in which triply degenerated and quadruply degenerated band crossings are reproduced at Γ and R points, respectively. The chiral fermions at Γ and R points also carry opposite topological charges. Without doping, the Fermi level is set to zero energy. With doping concentration of one electron (hole) per unit cell, the Fermi level shifts to the position of the higher (lower) red dashed line. Without doping, the calculated plasma frequency is 1.39 eV, and the calculated dielectric function $\epsilon(\omega)$ is shown in Fig. 2(b). The complex index of refraction $N = n(\omega) + ik(\omega)$ is shown in the inset of Fig. 2(b). In the range of low frequency, the real parts of $\epsilon(\omega)$ and N are very high because of the dominating intraband contribution. The calculated refractivity $n(\omega)$ is about

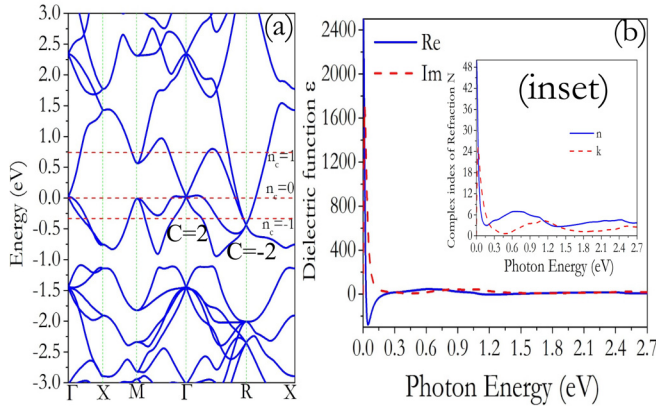


FIG. 2. The band structure of RhSi crystal without SOC, where the doping concentration n_c -dependent Fermi level is marked by a red dashed line. Without doping, the Fermi level is set to 0 eV. The chiral fermions at Γ on Fermi level and the R point below Fermi level have opposite chirality. With electron (hole) doping concentration $n_c = 1$ ($n_c = -1$), the Fermi level shifts to the higher (lower) red dashed line. (b) Frequency-dependent dielectric function $\epsilon(\omega)$ and complex refractive index $N = n(\omega) + ik(\omega)$ (inset) by the first-principles calculation within linear response. The peak at low frequency is dominated by the intraband contribution (Drude term).

51, which is very close to the experimental result [24]. Additionally, the extinction coefficient (or attenuation index) $k(\omega)$ is also very high in the range of low frequency, indicating high absorption and rapid attenuation when the optical field propagates through the chiral RhSi crystal. Since chiral crystal RhSi is nonmagnetic, time-reversal invariant symmetry is preserved. Therefore, the second-order Ohm conductivity is vanishing. Within the sum-over-state approximation, the calculated frequency-dependent electro-optical susceptibility tensor $\chi_{xyz}^{(2)}(\omega; \omega, 0)$ of RhSi contributed by shift current defined in Eq. (4) is shown in Fig. 3(a). At photon energies of 0.1 and 1.1 eV, the absolute value of the electro-optical

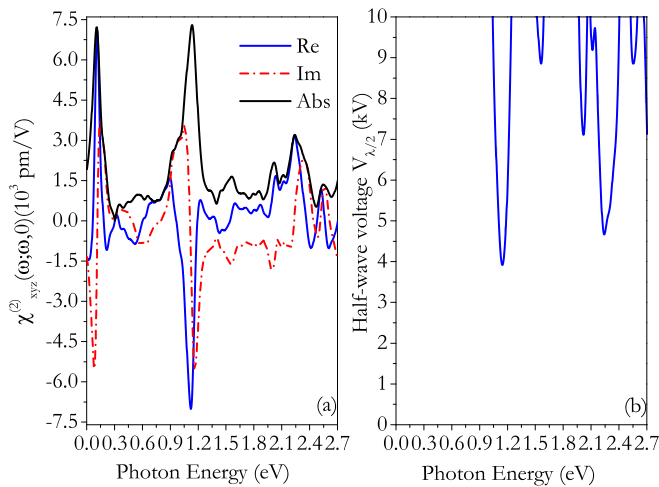


FIG. 3. (a) Frequency-dependent electro-optic coefficient $\chi_{xyz}^{(2)}(\omega; \omega, 0)$ contributed by the shift current, where the real and imaginary parts are plotted by a blue line and a red dash-dotted line, respectively. (b) Half-wave voltage determined by Eq. (11). At low frequency, the half-wave voltage is very high and out of range.

coefficient is as large as 7000 pm/V, which is much larger than that in the widely used electro-optic crystal LiNbO₃ [28]. We note that the second peak around 1.1 eV is very close to the O band (1260–1360 nm) of the second telecom window. With photon energy higher than 2.7 eV, there is no higher peak [54]. The calculated half-wave voltage by Eq. (11) is shown in Fig. 3(b), which shows relatively large voltage is required to achieve a phase difference of π between the two orthogonal optical fields $\frac{1}{\sqrt{2}}|E(\omega)|(1, \pm 1)$. The half-wave voltage is about 5 kV for visible light.

Since the CPGE in the chiral topological semimetal RhSi is observed in an energy window below 0.65 eV [24–26], and the CPGE coefficient is approximately proportional to topological charge, it means that only the chiral fermion at Γ is excited, while the chiral fermion at R below the Fermi level is far off resonance. This constraint reins in the frequency of the optical signal for communication. The frequency of the optical signal can be promoted if the pair of chiral fermions with opposite chirality is far separated in energy scale. With $\tau = 6.6$ fs [58] and $\chi = 2$, the calculated $|\sigma_{xyz}^{(2)}|$ from both injection current and nonlinear anomalous current is 86.2 $\mu\text{A}/\text{V}^2$ at 0.65 eV. With calculated $n = 6.97$, the calculated half-wave voltage at 0.65 eV is about 1350 V, which is much smaller than the half-wave voltage under the shift current mechanism, but still higher than the driving voltage of the CMOS circuit which is usually less than 3 V. For single crystal with high quality, the relaxation time can be 20 fs [59], and the half-wave voltage is reduced to about 445 V. To adapt to the CMOS circuit, the relaxation time should be further enhanced to reduce the half-wave voltage. Since the $|\sigma_{xyz}^{(2)}|$ is related to the Chern number, this coefficient can be further enhanced in chiral topological semimetals with higher Chern number. However, the relatively high extinction coefficient $k(\omega)$ of chiral topological semimetal RhSi means rapid attenuation when light propagates in the chiral crystal RhSi. Therefore, the thickness L of the electro-optic crystal defined in Eq. (10) should be as small as possible if the linear electro-optic effect is exploited to modulate the phase velocity of the light signal. Similar to a graphene-based electroabsorption modulator [36], RhSi can also be used as the metal in a metal-oxide-semiconductor capacitor in which the Fermi level of RhSi can be tuned by an electric signal [54]. This chiral crystal RhSi-based electroabsorption modulator can perform intensity modulation of the optical signal. Overall, chiral crystal RhSi can be used as both phase and intensity modulation because of its giant linear electro-optic coefficient and optical absorption.

V. SUMMARY

We identify that the linear electro-optic effect in chiral topological semimetals is dominated by oscillating nonlinear anomalous current and injection current, instead of shift current which dominates the linear electro-optic effect in semiconducting materials. The nonlinear optical conductivity $\sigma_{xyz}^{(2)}(\omega)$ contributed by the nonlinear anomalous current is antisymmetric under the exchange of indices x and y , and it is proportional to relaxation time and Chern number. With longer relaxation time or larger Chern number, the curvature involved currents can be significantly enhanced, and renders a relatively low half-wave voltage for phase modulation. This

work classifies how the Berry curvature modifies the linear electro-optic effect in chiral topological semimetals and opens an avenue to design the electro-optic modulator with half-wave voltage compatible with the CMOS circuit.

ACKNOWLEDGMENTS

This work was supported by the National Natural Science Foundation of China under Grant No. 61835013. Y.G. is

supported by National Key R&D Program of China (Grant No. 2017YFA0305500) and Natural Science Foundation of Jiangsu Province (Grant No. BK20200071). T.I. is supported by MEXT via Exploratory Challenge on Post-K Computer (Frontiers of Basic Science: Challenging the Limits). The calculations were performed on the Hokusai system (Project No. Q21246) of Riken. The authors are grateful to A. V. Pronin for sharing the original data of optical conductivity and for helpful discussion.

-
- [1] S. Geller and E. A. Wood, *Acta Crystallogr.* **7**, 441 (1954).
- [2] B. Q. Lv, T. Qian, and H. Ding, *Rev. Mod. Phys.* **93**, 025002 (2021).
- [3] N. P. Armitage, E. J. Mele, and A. Vishwanath, *Rev. Mod. Phys.* **90**, 015001 (2018).
- [4] J. Orenstein, J. E. Moore, T. Morimoto, D. H. Torchinsky, J. W. Harter, and D. Hsieh, *Annu. Rev. Condens. Matter Phys.* **12**, 247 (2021).
- [5] G. Chang, B. J. Wieder, F. Schindler, D. S. Sanchez, I. Belopolski, S.-M. Huang, B. Singh, D. Wu, T.-R. Chang, T. Neupert *et al.*, *Nat. Mater.* **17**, 978 (2018).
- [6] D. Takane, Z. Wang, S. Souma, K. Nakayama, T. Nakamura, H. Oinuma, Y. Nakata, H. Iwasawa, C. Cacho, T. Kim *et al.*, *Phys. Rev. Lett.* **122**, 076402 (2019).
- [7] G. Chang, S.-Y. Xu, B. J. Wieder, D. S. Sanchez, S.-M. Huang, I. Belopolski, T.-R. Chang, S. Zhang, A. Bansil, H. Lin, and M. Z. Hasan, *Phys. Rev. Lett.* **119**, 206401 (2017).
- [8] P. Tang, Q. Zhou, and S.-C. Zhang, *Phys. Rev. Lett.* **119**, 206402 (2017).
- [9] Z. Rao, H. Li, T. Zhang, S. Tian, C. Li, B. Fu, C. Tang, L. Wang, Z. Li, W. Fan *et al.*, *Nature (London)* **567**, 496 (2019).
- [10] D. S. Sanchez, I. Belopolski, T. A. Cochran, X. Xu, J.-X. Yin, G. Chang, W. Xie, K. Manna, V. Süß, C.-Y. Huang *et al.*, *Nature (London)* **567**, 500 (2019).
- [11] N. B. M. Schröter, D. Pei, M. G. Vergniory, Y. Sun, K. Manna, F. de Juan, J. A. Krieger, V. Süß, M. Schmidt, P. Dudin *et al.*, *Nat. Phys.* **15**, 759 (2019).
- [12] N. B. M. Schröter, S. Stolz, K. Manna, F. de Juan, M. G. Vergniory, J. A. Krieger, D. Pei, T. Schmitt, P. Dudin, T. K. Kim *et al.*, *Science* **369**, 179 (2020).
- [13] L. Z. Maulana, Z. Li, E. Uykur, K. Manna, S. Polatkan, C. Felser, M. Dressel, and A. V. Pronin, *Phys. Rev. B* **103**, 115206 (2021).
- [14] L. E. Golub and E. L. Ivchenko, *Phys. Rev. B* **98**, 075305 (2018).
- [15] E. Deyo, L. E. Golub, E. L. Ivchenko, and B. Spivak, [arXiv:0904.1917](https://arxiv.org/abs/0904.1917).
- [16] A. Cortijo, *Phys. Rev. B* **94**, 235123 (2016).
- [17] Z. Li, S. Zhang, T. Tohyama, X. Song, Y. Gu, T. Iitaka, H. Su, and H. Zeng, *Sci. China, Ser. G: Phys., Mech. Astron.* **64**, 107211 (2021).
- [18] Y. Gao, T. Iitaka, and Z. Li, *Eur. Phys. J. B* **94**, 95 (2021).
- [19] Z. Li, T. Iitaka, H. Zeng, and H. Su, *Phys. Rev. B* **100**, 155201 (2019).
- [20] F. de Juan, A. G. Grushin, T. Morimoto, and J. E. Moore, *Nat. Commun.* **8**, 15995 (2017).
- [21] Y. Zhang, H. Ishizuka, J. van den Brink, C. Felser, B. Yan, and N. Nagaosa, *Phys. Rev. B* **97**, 241118(R) (2018).
- [22] F. Flicker, F. de Juan, B. Bradlyn, T. Morimoto, M. G. Vergniory, and A. G. Grushin, *Phys. Rev. B* **98**, 155145 (2018).
- [23] C. Le, Y. Zhang, C. Felser, and Y. Sun, *Phys. Rev. B* **102**, 121111(R) (2020).
- [24] D. Rees, K. Manna, B. Lu, T. Morimoto, H. Borrmann, C. Felser, J. E. Moore, D. H. Torchinsky, and J. Orenstein, *Sci. Adv.* **6**, eaba0509 (2020).
- [25] A. Avdoshkin, V. Kozii, and J. E. Moore, *Phys. Rev. Lett.* **124**, 196603 (2020).
- [26] D. Rees, B. Lu, Y. Sun, K. Manna, R. Özgür, S. Subedi, H. Borrmann, C. Felser, J. Orenstein, and D. H. Torchinsky, *Phys. Rev. Lett.* **127**, 157405 (2021).
- [27] G. Sinatkas, T. Christopoulos, O. Tsilipakos, and E. E. Kriezis, *J. Appl. Phys.* **130**, 010901 (2021).
- [28] R. W. Boyd, *Nonlinear Optics* (Academic, Cambridge, 2003).
- [29] M. Li, J. Ling, Y. He, U. A. Javid, S. Xue, and Q. Lin, *Nat. Commun.* **11**, 4123 (2020).
- [30] C. Wang, M. Zhang, X. Chen, M. Bertrand, A. Shams-Ansari, S. Chandrasekhar, P. Winzer, and M. Lončar, *Nature (London)* **562**, 101 (2018).
- [31] R. Soref and B. Bennett, *IEEE J. Quantum Electron.* **23**, 123 (1987).
- [32] A. Liu, R. Jones, L. Liao, D. Samara-Rubio, D. Rubin, O. Cohen, R. Nicolaescu, and M. Paniccia, *Nature (London)* **427**, 615 (2004).
- [33] Q. Xu, B. Schmidt, S. Pradhan, and M. Lipson, *Nature (London)* **435**, 325 (2005).
- [34] C. Haffner, D. Chelladurai, Y. Fedoryshyn, A. Josten, B. Baeuerle, W. Heni, T. Watanabe, T. Cui, B. Cheng, S. Saha *et al.*, *Nature (London)* **556**, 483 (2018).
- [35] M. Ayata, Y. Fedoryshyn, W. Heni, B. Baeuerle, A. Josten, M. Zahner, U. Koch, Y. Salamin, C. Hoessbacher, C. Haffner *et al.*, *Science* **358**, 630 (2017).
- [36] M. Liu, X. Yin, E. Ulin-Avila, B. Geng, T. Zentgraf, L. Ju, F. Wang, and X. Zhang, *Nature (London)* **474**, 64 (2011).
- [37] C. T. Phare, Y.-H. D. Lee, J. Cardenas, and M. Lipson, *Nat. Photonics* **9**, 511 (2015).
- [38] K. Chen, X. Zhou, X. Cheng, R. Qiao, Y. Cheng, C. Liu, Y. Xie, W. Yu, F. Yao, Z. Sun *et al.*, *Nat. Photonics* **13**, 754 (2019).
- [39] J. E. Sipe and A. I. Shkrebtii, *Phys. Rev. B* **61**, 5337 (2000).
- [40] X.-L. Zhang, L.-F. Liu, and W.-M. Liu, *Sci. Rep.* **3**, 2908 (2013).
- [41] Z. Li, J. Kim, N. Kioussis, S.-Y. Ning, H. Su, T. Iitaka, T. Tohyama, X. Yang, and J.-X. Zhang, *Phys. Rev. B* **92**, 201303(R) (2015).

- [42] T. Zhang, J.-H. Lin, Y.-M. Yu, X.-R. Chen, and W.-M. Liu, *Sci. Rep.* **5**, 13927 (2015).
- [43] F. Sun, T. Zhang, C. J. Yi, Y. L. Wu, H. Zhao, Q. Wu, Y. G. Shi, H. Weng, and J. Zhao, *Phys. Rev. B* **104**, L100301 (2021).
- [44] A. Taghizadeh, F. Hipolito, and T. G. Pedersen, *Phys. Rev. B* **96**, 195413 (2017).
- [45] Z. Li, Y.-Q. Jin, T. Tohyama, T. Iitaka, J.-X. Zhang, and H. Su, *Phys. Rev. B* **97**, 085201 (2018).
- [46] Y.-Q. Ma, S. Chen, H. Fan, and W.-M. Liu, *Phys. Rev. B* **81**, 245129 (2010).
- [47] M. Kolodrubetz, D. Sels, P. Mehta, and A. Polkovnikov, *Phys. Rep.* **697**, 1 (2017).
- [48] A. Graf and F. Piéchon, *Phys. Rev. B* **104**, 085114 (2021).
- [49] P. Bhalla, K. Das, D. Culcer, and A. Agarwal, [arXiv:2108.04082](https://arxiv.org/abs/2108.04082).
- [50] J. Ahn, G.-Y. Guo, and N. Nagaosa, *Phys. Rev. X* **10**, 041041 (2020).
- [51] T. Morimoto and N. Nagaosa, *Sci. Adv.* **2**, e1501524 (2016).
- [52] I. Sodemann and L. Fu, *Phys. Rev. Lett.* **115**, 216806 (2015).
- [53] Z. Z. Du, H.-Z. Lu, and X. C. Xie, *Nat. Rev. Phys.* **3**, 744 (2021).
- [54] See Supplemental Material at <http://link.aps.org/supplemental/10.1103/PhysRevB.105.125201> for detailed derivations of linear and nonlinear optical conductivity with dipole approximation, and the calculated optical conductivity, electro-optic coefficient in large photon energy scale.
- [55] E. Sjöstedt, L. Nordström, and D. J. Singh, *Solid State Commun.* **114**, 15 (2000).
- [56] X. Gonze, F. Jollet, F. A. Araujo, D. Adams, B. Amadon, T. Applencourt, C. Audouze, J.-M. Beuken, J. Bieder, and A. Bokhanchuk *et al.*, *Comput. Phys. Commun.* **205**, 106 (2016).
- [57] S. Sharma and C. Ambrosch-Draxl, *Phys. Scr.* **T109**, 128 (2004).
- [58] Z. Ni, B. Xu, M.-Á. Sánchez-Martínez, Y. Zhang, K. Manna, C. Bernhard, J. W. F. Venderbos, F. de Juan, C. Felser, A. G. Grushin, and L. Wu, *npj Quantum Mater.* **5**, 96 (2020).
- [59] L. Z. Maulana, K. Manna, E. Uykur, C. Felser, M. Dressel, and A. V. Pronin, *Phys. Rev. Research* **2**, 023018 (2020).